-Supporting Information-
Conical Intersection Passages of Molecules Probed by X-ray Diffraction and Stimulated Raman Spectroscopy

Yeonsig Nam[*,a,b], Daniel Keefer[a], Artur Nenov[c], Irene Conti[c], Flavia Aleotti[c],

Francesco Segatta[c], Jin Yong Lee[*,b,d], Marco Garavelli[c], and Shaul Mukamel[*,a]

[a]Department of Chemistry, University of California, Irvine, California 92697-2025, United States
[b]Convergence Research Center for Energy and Environmental Sciences, Sungkyunkwan University, Suwon 16419, Korea
[c]Dipartimento di Chimica Industriale "Toso Montanari," Universita' degli Studi di Bologna, I-40136 Bologna, Italy

[d]Department of Chemistry, Sungkyunkwan University, Suwon 16419, Korea
[*]yeonsign@uci.edu, jinylee@skku.edu, smukamel@uci.edu

September 3, 2021

Contents

1 Signal Derivation

1.1 Off-Resonant TRUECARS Signal

The TRUECARS technique involves stimulated X-ray Raman process: A narrowband $\mathcal{E}_N$ pulse excites the system, and broadband $\mathcal{E}_B$ pulse stimulates the emission of the photon. The associated loop diagram is shown in Sch. 1b in the main manuscript. The off-resonant stimulated Raman process, in the rotating wave approximation, is described by the following multipolar light-matter interaction Hamiltonian [1]

$$H_{\text{int}} = -\alpha(\mathcal{E}_B^\dagger \mathcal{E}_N + \mathcal{E}_N^\dagger \mathcal{E}_B) \tag{S1}$$

where α is the electronic polarizability operator, and $\mathcal{E}_{N/B}$ are narrowband/broadband electric-field operator, respectively:

$$\mathcal{E}_{B/N} = i \sum_s \sqrt{\frac{2\pi\omega_s}{V}} \epsilon_s a_s e^{ik_s r} \tag{S2}$$

V is the quantization volume, and $a_s^{(\dagger)}$ are the annihilation (creation) operators of a photon with frequency ω_s, respectively. The Raman interaction from the broadband $\mathcal{E}_B^\dagger \mathcal{E}_B$ or the narrowband $\mathcal{E}_N^\dagger \mathcal{E}_N$ also contribute to the signal, but is neglected in our model Hamiltonian. The narrow/broadband single probe pulse do not provide a temporal/spectral resolution of the hybrid scheme. In the presence of pump and probe pulses, one can assume that the pump pulse is more intense than the probe pulse. In this case, the $\mathcal{E}_N^\dagger \mathcal{E}_B$ or $\mathcal{E}_B^\dagger \mathcal{E}_N$ interaction will be stronger than the $\mathcal{E}_N \mathcal{E}_N$ or $\mathcal{E}_B \mathcal{E}_B$ and one can neglect this weak latter contributions. The TRUECARS signal is defined in terms of the frequency-resolved probe pulse intensity after passing through the sample. Hence, it is given by the time-integrated rate of change of the number of photons of frequency ω_s in the $\mathcal{E}_B$ pulse

$$S(k_s) = \int dt \left\langle \frac{d}{dt} N_s^B \right\rangle \tag{S3}$$

where $N_s^B = a_s^\dagger a_s$ is the number operator of a photon with the detected signal frequency ω_s, stimulately emitted by $\mathcal{E}_B$ pulse. The signal is calculated by propagating Heisenberg equations of motion for photon number operator, via the commutator $[H_{\text{int}}, N_s^B]$. We use classical electric fields,

$$\mathcal{E}_N = \mathcal{E}_N(t-T)e^{-i\omega_s(t-T)}e^{i\phi_N} \qquad\qquad \mathcal{E}_B = \mathcal{E}_B(\omega_s)e^{i\phi_B} \tag{S4}$$

where $\mathcal{E}_{B/N}$ are envelope function with carrier frequency ω_s, centered at the time delay T. We match the phase of narrowband and broadband pulse so that ($\phi_B = \phi_N$), then the off-resonant TRUECARS signal becomes

$$S(\omega_s, T) = 2\text{Im} \int dt e^{-i\omega_s(t-T)} \mathcal{E}_B(\omega_s)^* \mathcal{E}_N(t-T)\langle \alpha(t)\rangle \tag{S5}$$

where 'Im' and 'Re' refer to imaginary and real part of the term. We expand the total time-dependent molecular wavefunction $\psi(r, R, t)$ in the adiabatic basis

$$\psi(r, R, t) = \sum_i c_i(t)\chi(R, t)\phi(r, R) \tag{S6}$$

where $\chi(\mathbf{R}, t)$ is the normalized nuclear wavepacket in the adiabatic electronic state $\phi(\mathbf{r}, \mathbf{R})$, and c_i is the coefficient (amplitude) of adiabatic states. We rewrite the expectation value $\langle ... \rangle$ in Eq. S5 explicitly in terms of the total (nuclear and electronic) wavefunction $|\psi(t)\rangle$

$$S(\omega_s, T) = 2\text{Im} \int dt e^{i\omega(t-T)} \mathcal{E}_B(\omega_s)^* \mathcal{E}_N(t-T) \langle \psi(t)|\boldsymbol{\alpha}|\psi(t)\rangle \tag{S7}$$

The minimal-coupling Hamiltonian [2] provides the complete formalism to describe the interaction between light and matter by avoiding the multipolar expansion. The effective light-matter interaction Hamiltonian in Eq. S1 and the polarizability operator therein can be expressed in terms of molecular charge- and current density operators. By discarding the resonant interaction term $\mathbf{j} \cdot \mathbf{A}$ [3],

$$H_{\text{int}} = \frac{1}{2} \int d\mathbf{r} \sigma(\mathbf{r}) \left(\mathcal{E}_B^\dagger(\mathbf{r})\mathcal{E}_N(\mathbf{r}) + \mathcal{E}_N^\dagger(\mathbf{r})\mathcal{E}_B(\mathbf{r}) \right) \tag{S8}$$

$$\boldsymbol{\alpha}_{\text{eff}}(t) = \int d\mathbf{r} \int d\mathbf{r}' \sigma(\mathbf{r}, t) e^{ik(\mathbf{r}-\mathbf{r}')} \tag{S9}$$

where $\sigma(\mathbf{r})$ term is the charge-density operator. Integrating over r and r' gives,

$$\langle \sigma(\mathbf{q}, t) \rangle = \int d\mathbf{r} e^{-i\mathbf{q}\mathbf{r}} \langle \sigma(\mathbf{r}, t) \rangle \tag{S10}$$

then, we recover the Eq. S5,

$$S(\omega_s, T) = \text{Im} \int dt e^{i\omega_s(t-T)} \mathcal{E}_B^*(\omega_s) \mathcal{E}_N(t-T) \langle \sigma(\mathbf{q}, t) \rangle \tag{S11}$$

showing that, in the minimal coupling, the transition polarizability in Eq. S5 is simply substituted by the transition charge densities. To get the TRUECARS signal, we computed effective polarizability value from transition charge density at 2450 eV. For example, the TRUECARS signal along z axis was calculated from the transition polarizability $\boldsymbol{\alpha}_{\text{eff}}(\mathbf{q}) = \sigma(\mathbf{q})$ at $q_x = 0, q_y = 0$, and $q_z = |k_z| = \omega_s/c$ for the total of 128×128 nuclear coordinates, where ω_s is the probe carrier frequency of 90.036 $a.u.$ and c is the speed of the light, 137.036 $a.u.$. By the same argument, TRUECARS signals along x, and y axes were computed and shown in Fig. S5.

1.2 Off-Resonant Diffraction Signal

We follow the derivation of off-resonant time-resolved X-ray diffraction (TXRD) in refs [4][5]. An incident photon is scattered from the molecular charge density $\sigma(\mathbf{q})$, where $\sigma(\mathbf{q})$ is the Fourier transform of the real-space charge density $\sigma(\mathbf{r})$. The scattering vector $\mathbf{q} = \mathbf{k}_s - \mathbf{k}_p$ represents the momentum transfer between incident ($\mathbf{k}_p$) and scattered ($\mathbf{k}_s$) photon. The molecular charge density $\sigma(\mathbf{q})$ is a single-body electron operator which parametrically depends on nuclear coordinate $\mathbf{R}$, i.e., $\sigma(\mathbf{q}, \mathbf{R})$. The single-molecule TXRD signal [4][5] of a sample with N noninteracting molecule is expressed by

$$S_1(\mathbf{q}, T) \propto N \int dt |\mathcal{E}_X(t-T)|^2 \tilde{S}_1(\mathbf{q}, t) \tag{S12}$$

with the time delay T, X-ray probe pulse envelope $\mathcal{E}_X(t - T)$ centered at time T, and the time-dependent molecular response $\tilde{S}_1(q, t)$. Using two electronic states (dark first excited state S_1 and the bright second excited state S_2), $\tilde{S}_1(q, t)$ reads

$$\tilde{S}_1(q, t)$$
$$= \rho_{S_1 S_1}(t)\langle \chi_{S_1}(t)|\sigma^\dagger_{S_1 S_1}\sigma_{S_1 S_1}|\chi_{S_1}(t)\rangle \tag{i}$$
$$+ \rho_{S_2 S_2}(t)\langle \chi_{S_2}(t)|\sigma^\dagger_{S_2 S_2}\sigma_{S_2 S_2}|\chi_{S_2}(t)\rangle \tag{ii}$$
$$+ \rho_{S_1 S_1}(t)\langle \chi_{S_1}(t)|\sigma^\dagger_{S_1 S_2}\sigma_{S_2 S_1}|\chi_{S_1}(t)\rangle \tag{iii}$$
$$+ \rho_{S_2 S_2}(t)\langle \chi_{S_2}(t)|\sigma^\dagger_{S_2 S_1}\sigma_{S_1 S_2}|\chi_{S_2}(t)\rangle \tag{iv}$$
$$+ 2\text{Re}[\rho_{S_2 S_1}(t)\langle \chi_{S_2}(t)|\sigma^\dagger_{S_2 S_2}\sigma_{S_2 S_1}|\chi_{S_1}(t)\rangle + \rho_{S_2 S_1}(t)\langle \chi_{S_2}(t)|\sigma^\dagger_{S_2 S_1}\sigma_{S_1 S_1}|\chi_{S_1}(t)\rangle] \tag{v}$$
$$\tag{S13}$$

where each term corresponds to a particular loop diagram in Fig. S7. Here we write $\sigma(q, R) = \sigma$ for brevity. $\rho_{S_1 S_1}$ and $\rho_{S_2 S_2}$ are the electronic state populations, $\rho_{S_1 S_2}$ is the coherence magnitude. Hence, the first (i) and the second (ii) term represent elastic scattering from the first and the second excited state, respectively. The third (iii) and fourth (iv) term describe inelastic scattering from both states. The last term (v) represents the mixed elastic/inelastic scattering from vibronic coherence. Note that our nuclear wavepacket does not decay to the ground state while it is absorbed at the S_1 minimum, hence we neglect the contribution from the ground state and consider only the contribution from S_1 and S_2 states.

2 Loop Diagram Rules

The loop diagram of the TRUECARS signal is shown in Sch. 1b in the main manuscript. The Diagram rules are as follows:

- Time runs along the loop clockwise from bottom left to bottom right.

- Each field interaction is represented by an arrow, which either points to the right (photon annihilation and excitation of the molecule) or to the left (photon creation and de-excitation of the molecule).

- Free evolution periods on the left branch indicate forward propagation in real time, and on the right branch to backward propagation respectively.

- The last field interaction (in this case, k_s) is the detected photon mode. In addition, the gray bar represents the period of free evolution.

3 Result and Discussion

Three-dimensional diffraction pattern and the projected diffraction signal integrating over q_x, q_y, or q_z are presented in Fig. S9 and S10, respectively. The total signals are dissected into the different contribution as labeled in Eq. 9. The dominant term is elastic scattering from population state: term (i) (excited state $\rho_{S_1 S_1}$) and term (ii) (excited state $\rho_{S_2 S_2}$) while the former being weaker than

the latter one since $\rho_{S_2 S_2}$ is larger than $\rho_{S_1 S_1}$. The inelastic scattering terms (iii)/(iv) are 2026/2127 times weaker than their elastic counterpart when comparing their maximal intensity. The S_1 population term (i) and (iii) first appear at 20 fs and repeat its (dis)appearance as the nuclear WP oscillate between the FC and the CoIn. Another S_2 population term (ii) and (iv) are nonvanishing at the beginning, become intensified till 25 fs and start to vanish as the population decays. By the same argument, the coherence contribution (v) is 2118 times weaker than the maximal intensity of the total signal showing similar strength to the inelastic terms. It first shows up at 20 fs when S_2 WP passes by area with finite NAC. The coherence term exhibits both positive (red) and negative (blue) contributions showing the phase oscillation when comparing at 30, 50, and 61 fs.

The ratio of the each scattering contribution to the total signal is shown in Fig. S12. The ratio becomes finite above 4 $\mathring{A}^{-1}$ for coherence contribution (v), and above 6 $\mathring{A}^{-1}$ for inelastic contributions (iii and iv). The ratio for coherence term goes up to 0.014 at 50 fs and 14 $\mathring{A}^{-1}$ compared to the total signal. The total number of electrons for 4TU (66 electrons) is smaller than that of azobenzene (96 electrons), hence the ratios of terms (iii) to (v) against the total signal are somewhat larger than those of azobenzene [6]. The terms (iii) to (v) which involve transition charge density $\sigma_{S_2 S_1}$ are more localized in the real-space thus being more spread in $\boldsymbol{q}$ space.

4 References

[1] Markus Kowalewski et al. "Catching Conical Intersections in the Act: Monitoring Transient Electronic Coherences by Attosecond Stimulated X-Ray Raman Signals". In: *Phys. Rev. Lett.* 115 (19 Nov. 2015), p. 193003. DOI: 10.1103/PhysRevLett.115.193003. URL: https://link.aps.org/doi/10.1103/PhysRevLett.115.193003.

[2] Jérémy R. Rouxel, Markus Kowalewski, and Shaul Mukamel. "Current vs Charge Density Contributions to Nonlinear X-ray Spectroscopy". In: *Journal of Chemical Theory and Computation* 12.8 (2016). PMID: 27347786, pp. 3959–3968. DOI: 10.1021/acs.jctc.6b00279. eprint: https://doi.org/10.1021/acs.jctc.6b00279. URL: https://doi.org/10.1021/acs.jctc.6b00279.

[3] Vladimir Y. Chernyak, Prasoon Saurabh, and Shaul Mukamel. "Non-linear non-local molecular electrodynamics with nano-optical fields". In: *The Journal of Chemical Physics* 143.16 (2015), p. 164107. DOI: 10.1063/1.4934231. eprint: https://doi.org/10.1063/1.4934231. URL: https://doi.org/10.1063/1.4934231.

[4] Kochise Bennett et al. "Monitoring molecular nonadiabatic dynamics with femtosecond X-ray diffraction". In: *Proceedings of the National Academy of Sciences* 115.26 (2018), pp. 6538–6547. ISSN: 0027-8424. DOI: 10.1073/pnas.1805335115. eprint: https://www.pnas.org/content/115/26/6538.full.pdf. URL: https://www.pnas.org/content/115/26/6538.

[5] Jérémy R. Rouxel, Daniel Keefer, and Shaul Mukamel. "Signatures of electronic and nuclear coherences in ultrafast molecular x-ray and electron diffraction". In: *Structural Dynamics* 8.1 (2021), p. 014101. DOI: 10.1063/4.0000043. eprint: https://doi.org/10.1063/4.0000043. URL: https://doi.org/10.1063/4.0000043.

[6] Daniel Keefer et al. "Imaging conical intersection dynamics during azobenzene photoisomerization by ultrafast X-ray diffraction". In: *Proceedings of the National Academy of Sciences* 118.3 (2021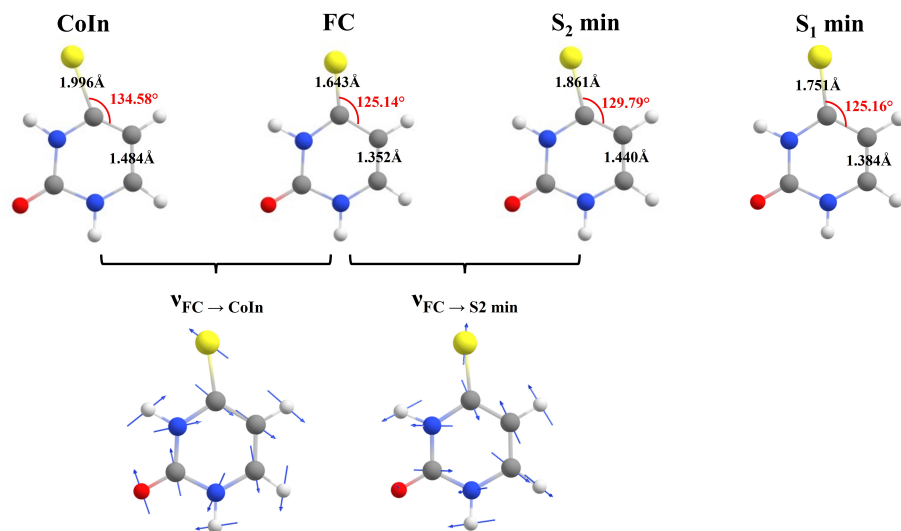). ISSN: 0027-8424. DOI: 10.1073/pnas.2022037118. eprint: https://www.pnas.org/content/118/3/e2022037118.full.pdf. URL: https://www.pnas.org/content/118/3/e2022037118.

5   Supplementary Figures

Fig. S 1: Optimized geometry for the ground state minimum (FC), $S_2 - S_1$ conical intersection (CoIn), the S_2 minimum (S_2 min), and the S_1 minimum (S_1 min) and the two coordinate vectors spanning two-dimensional coordinates. The C=S and C=C bond lengths are presented in black and the $\angle$CCS is presented in red.
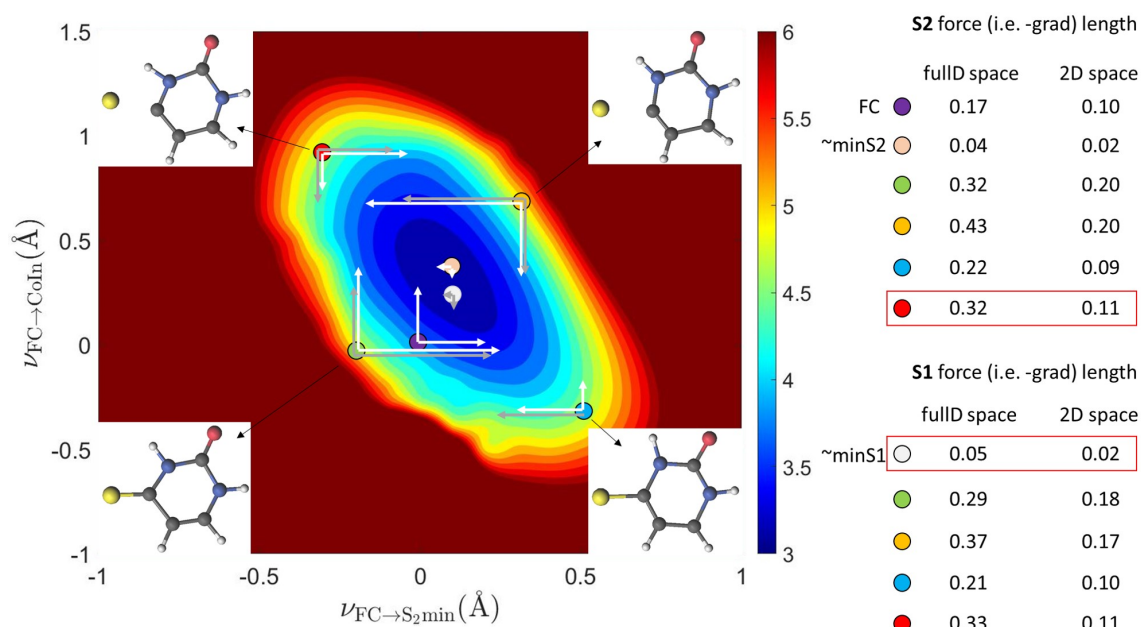
Fig. S 2: The projection of the S_2 (white arrows) and S_1 (grey arrows) gradient on the reactive coordinates. The purple, light pink, and white circle represent the location of the FC, the S_2 min, and the S_1 min, respectively. The four molecular structures at the edges represents the geometry at the other points (red, green, blue, and orange circles). The table represents the length of the vectors in full three-dimensional space and of the projection at the given points.
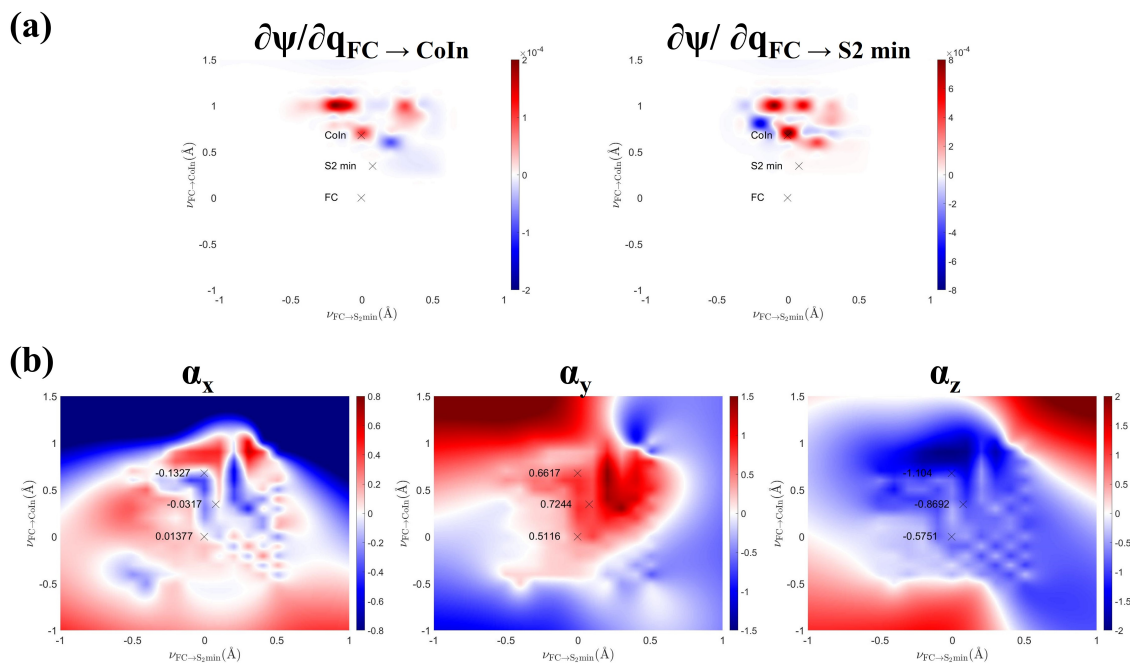
(a)

(b)

Fig. S 3: (a) Nonadiabatic couplings versus the two nuclear coordinates of the molecules. The location of the FC, CoIn, and S_2 min are marked with X. (b) $S_2 - S_1$ transition probabilities at 2450 eV. The transition polarizability values are given for the location of the FC, CoIn, and S_2 min (marked with X).
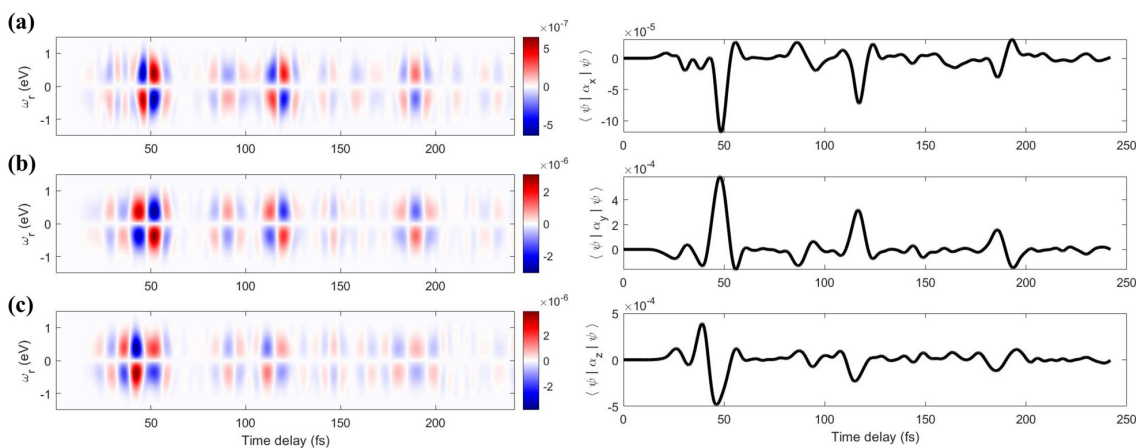

Fig. S 5: Comparison of molecular orientation in the TRUECARS signal along a) x (α_x), (b) y (α_y), and (c) z (α_z) axis. The y and z component exhibits stronger signal than the x component. The left figures show the TRUECARS signal and the right figrues show the expectation value of the polarizability operator for each direction
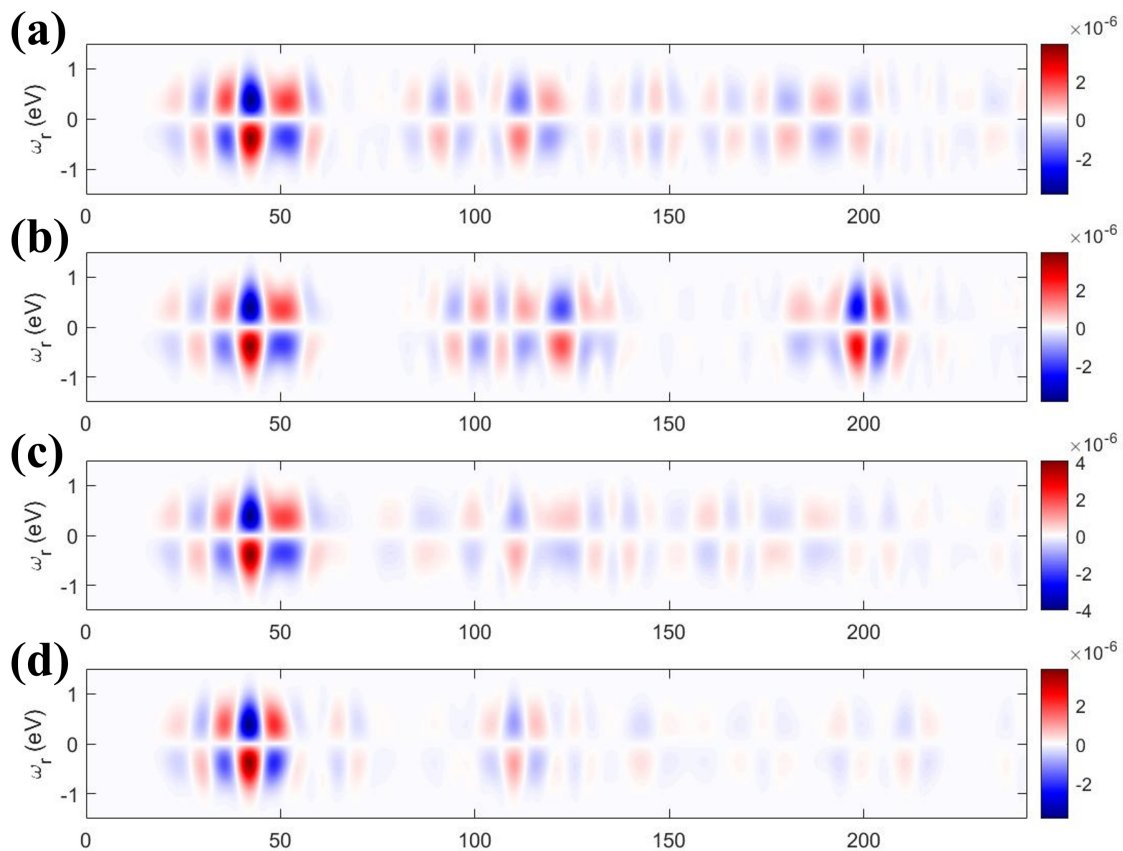
S10

(a)

(b)

(c)

(d)

Fig. S 6: The TRUECARS signal along z axis at the different placement of Gobblers. $\nu_{FC \to CoIn} =$ (a) -0.1 (near S_1 min), (b) -1.0 (far below S_1 min), (c) 0.55, and (d) 1.0.

S11

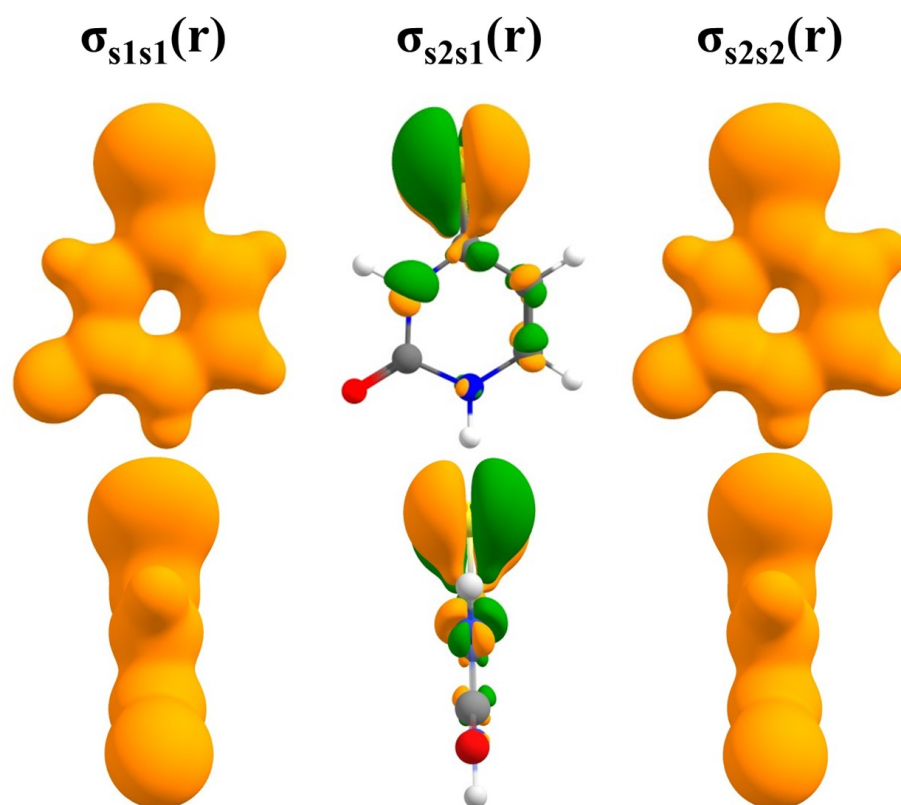$$\sigma_{s1s1}(r) \qquad \sigma_{s2s1}(r) \qquad \sigma_{s2s2}(r)$$

Fig. S 7: Real-space charge densities of 4TU at the conical intersection geometry (isovalue 0.025 for $\sigma_{S_1 S_1}$ and $\sigma_{S_2 S_2}$, 0.0025 for $\sigma_{S_2 S_1}$)
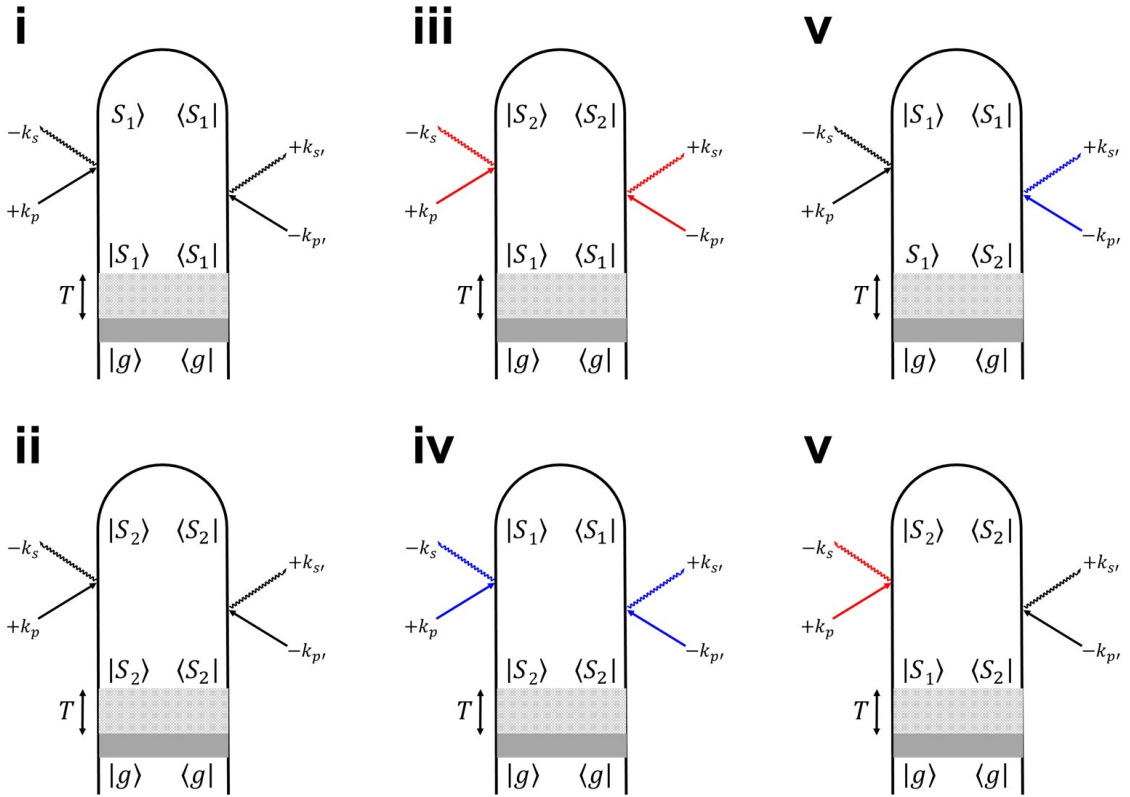
Fig. S 8: Loop diagrams for single-molecule X-ray scattering process. The shaded area represents an excitation that prepares the system in $|S_2\rangle$ state. The checkered box represents a field-free nonadiabatic dynamics during time delay T. We denote modes of the X-ray probe pulse with p and p', whereas s and s' represent relevant scattering modes. Elastic scattering process are denoted by black field arrows. Inelastic processes are denoted by red (stokes) or blue (anti-stoke) arrows.
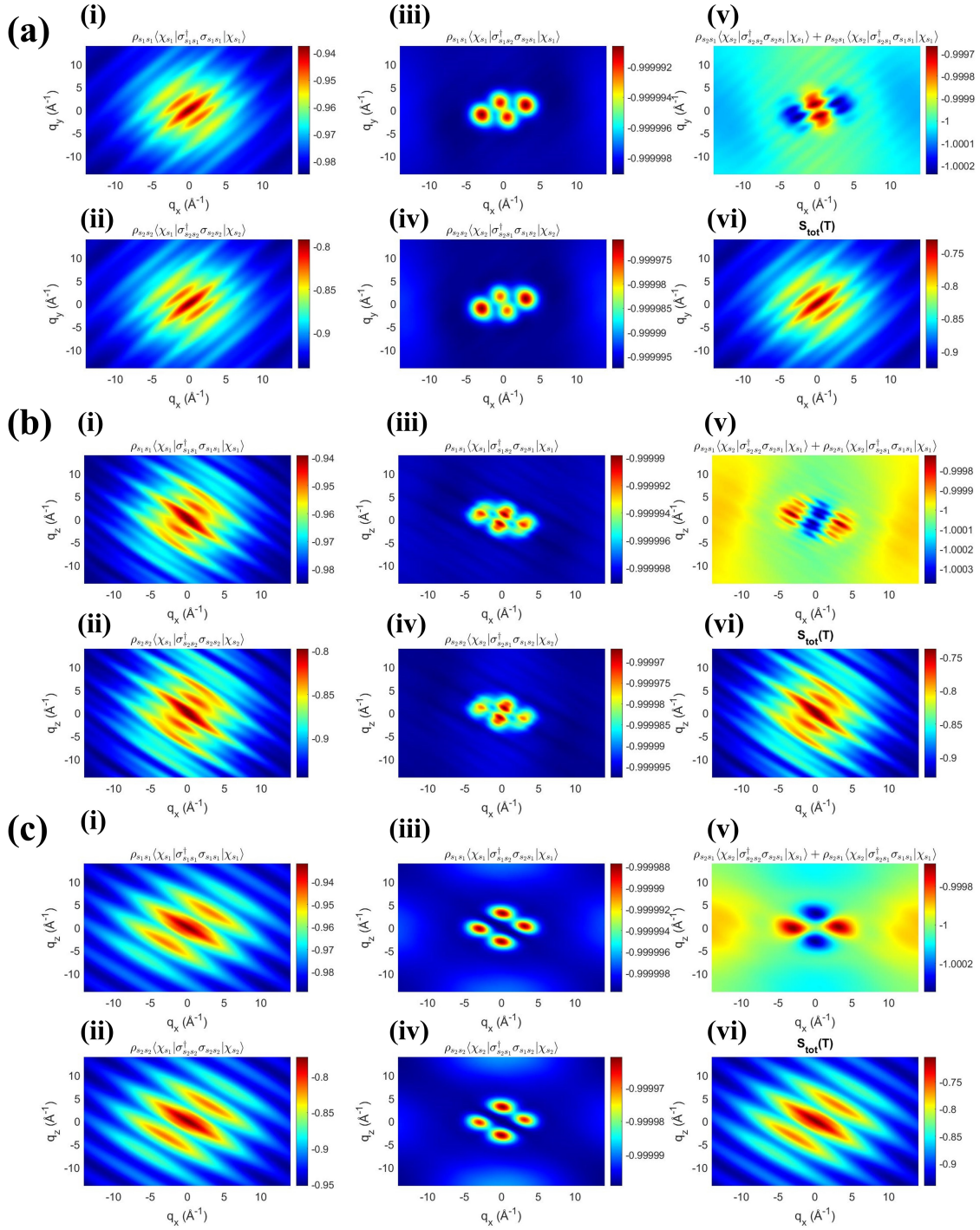
Fig. S 10: Normalized two-dimensional diffraction patterns in the (a) q_{xy}, (b) q_{xz}, and (c) q_{yz} planes, after integrating over the respective other direction at 45 fs. Each term is labeled according to Eq. 9.
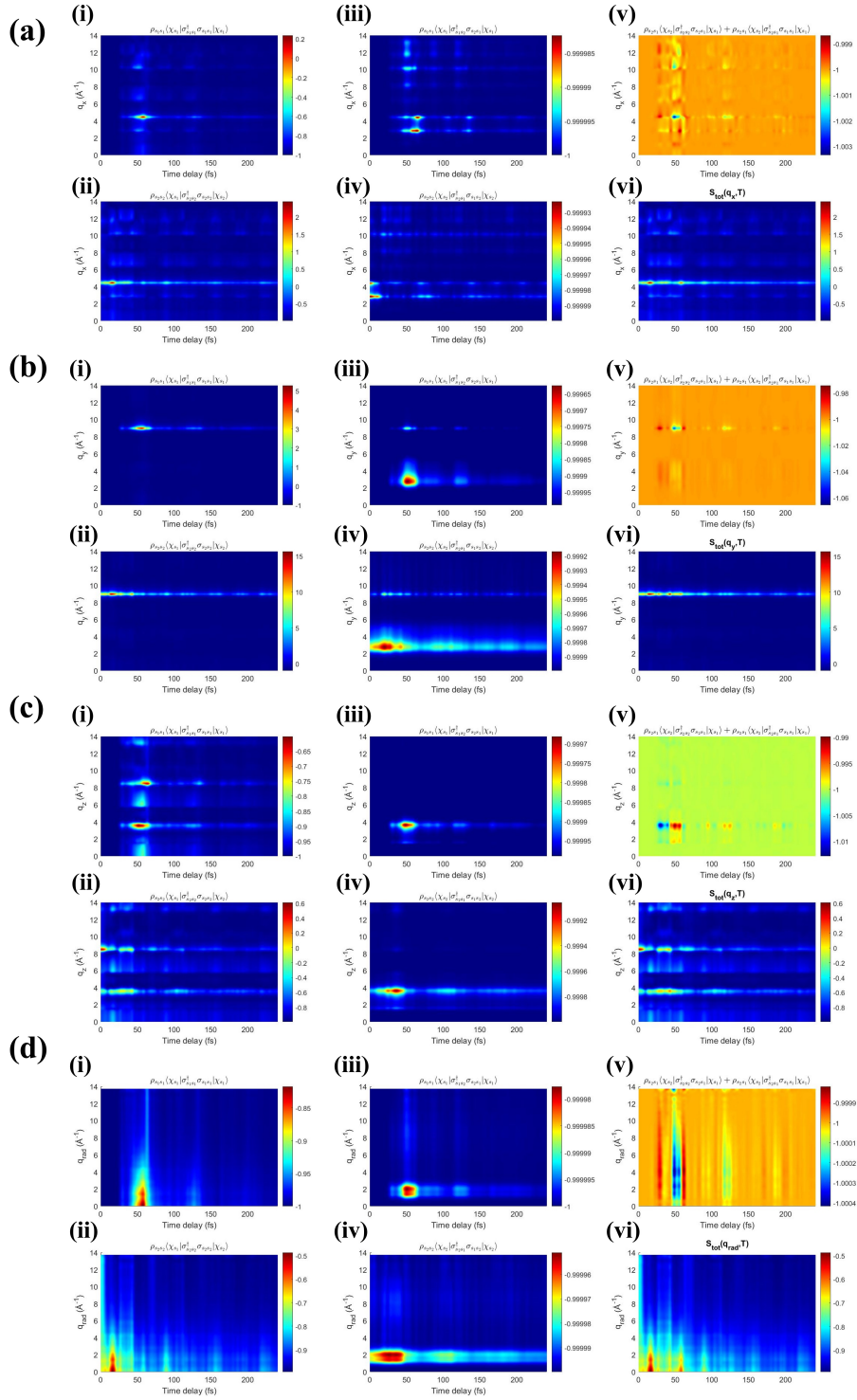
Fig. S 11: Normalized time-resolved diffraction signal $S(\boldsymbol{q}, T)$ along (a)$\boldsymbol{q}_x$, (b)$\boldsymbol{q}_y$, (c)$\boldsymbol{q}_z$, and (d)$\boldsymbol{q}_{rad}$ directions.
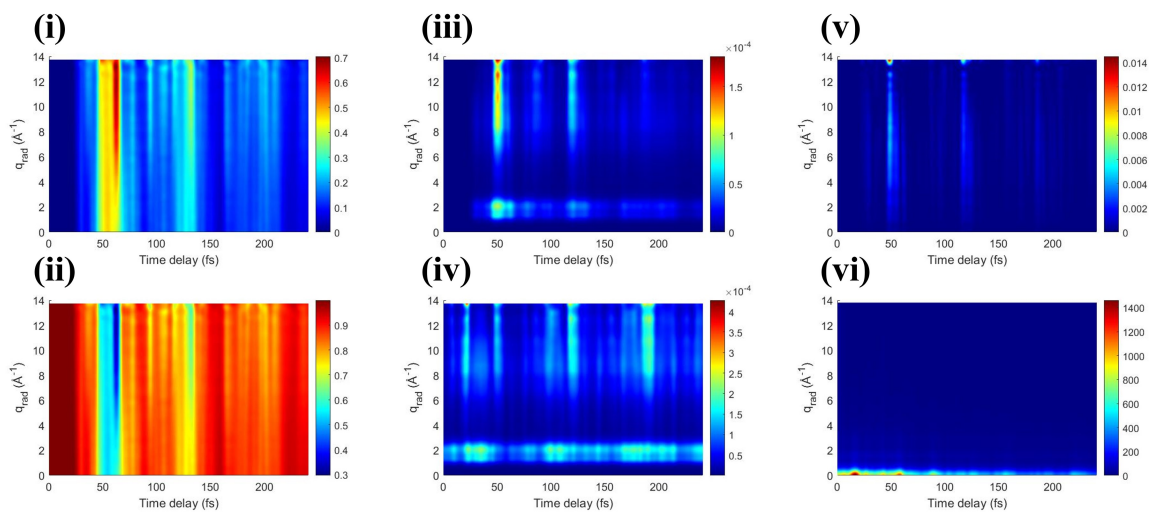
Fig. S 12: (i)-(v) Ratio of the strength of each contribution (labeled according to Eq. 9) in Fig. S10d vs in the total signal (vi).